

## Predicting the Timing of the the Solar Cycle 25 Polar Field Reversal

BIBHUTI KUMAR JHA <sup>1</sup> AND LISA A. UPTON <sup>1</sup>

<sup>1</sup>*Southwest Research Institute, Boulder, CO 80302, USA*

(Received October 13, 2023; Accepted January 22, 2024)

### ABSTRACT

The process of the Sun’s polar field cancellation reversal commences with the emergence of new cycle Hale’s polarity active regions. Once the Sun undergoes polarity reversal, typically occurring near the peak of solar activity, it begins the process of accumulating the seed field for the forthcoming solar cycle. In recent years, the Advective Flux Transport (AFT) model has proven highly effective in forecasting the progression of polar fields by leveraging observations of surface flows and magnetic flux emergence. In this study, we make use of the predictive capability of the AFT model to simulate the evolution of the polar fields and estimate the timing of the Solar Cycle 25 polarity reversal in both hemispheres of the Sun. We use the statistical properties of active regions along with Solar Cycle 13, which closely resembles the current solar cycle (Cycle 25), to generate synthetic active regions in order to simulate future magnetic flux emergence in AFT to predict the evolution of the polar field. Based on our simulations, we anticipate that the Northern hemisphere of the Sun will undergo a polarity reversal between June 2024 and November 2024, with the center of our distribution at August 2024. In the Southern hemisphere, we anticipate a polarity reversal between November 2024 and July 2025, centered around February 2025. Additionally, assuming that the reversal of the axial dipole moment coincides with the peak of the solar cycle, our findings indicate that Cycle 25 is expected to peak in 2024 (likely between April to August 2024).

*Keywords:* Sunspot (1653) — Solar Cycle (1487) — Solar magnetic flux emergence(2000) — Solar magnetic fields (1503)

### 1. INTRODUCTION

Understanding solar activity cycle variability has been a persistent problem in the field of solar physics. Despite over a century of dedicated solar observations, this puzzle has yet to be resolved and our understanding of the solar activity cycle remains incomplete (see [Bhowmik et al. 2023](#)). The intimate relation between the solar cycle and the polar field of the Sun was first suggested by [Babcock \(1959\)](#) and put forward by [Babcock \(1961\)](#) as the foundation of solar dynamo models (see [Charbonneau 2010](#), for extensive review on the dynamo models). The amplitude of the polar field at the beginning of the solar cycle acts as the seed field for the upcoming cycle and is one of the best proxies for predicting the strength

of following solar cycle ([Svalgaard et al. 2005](#); [Hathaway 2010](#); [Muñoz-Jaramillo et al. 2012](#); [Svalgaard & Kamide 2013](#); [Upton & Hathaway 2023](#)). The reversal of the polar field occurs close to cycle maximum ([Babcock 1959](#)), beginning the creation of the seed field for the upcoming cycle ([Golubeva et al. 2023](#)).

In the last few decades, Surface Flux Transport (SFT; [DeVore et al. 1984](#); [Wang et al. 1989](#); [van Ballegoijen et al. 1998](#); [Schrijver & Title 2001](#); [Bhowmik & Nandy 2018](#)) models have been exceptionally successful in simulating observed solar cycle behavior. SFT models illustrate how residual flux from tilted active regions (ARs) is carried to the poles by the meridional flow, leading to the cancellation of the existing polar field and the build up of the new polar field. However, the chaotic nature of the AR emergence and their tilts ([Jha et al. 2020](#)) poses a challenge for models operating in a predictive mode. Without advance knowledge of future flux emergence,

it is difficult to accurately predict the evolution of the polar field.

A recent advancement in SFT modeling is the development of the Advective Flux Transport (Upton & Hathaway 2014a,b, AFT;) model. AFT uses the observed flows on the Sun’s surface, as opposed to parameterized flows. For example, diffusion is typically used in other SFT models to mimic the effects of convection (Jiang et al. 2014; Bhowmik & Nandy 2018; Yeates et al. 2023), however AFT uses a convective simulation to explicitly incorporate the effects of the convective motions. AFT has proven successful in modeling the polar field evolution (e.g., obtaining an excellent match with the observed polar field from Wilcox Solar Observatory (WSO) and Helioseismic Magnetic Imager (HMI; Scherrer et al. 2012; Sun et al. 2015), and has been reliable in predicting the timing of the Sun’s polar field reversals (Upton & Hathaway 2014a,b; Hathaway & Upton 2016).

We are approaching the maxima of the current cycle (Solar Cycle 25) and the polarity reversal of the Sun’s magnetic dipole is imminent. The evolution of the polar field in the near future is a marker for solar activity in the coming years, as we can expect the waning of solar activity after the reversal of polar fields. Knowing the level of solar activity in coming years is important for forecasting our space weather environment and ensuring the safety of our space technology and communication systems. In this letter we use the predictive capability of the AFT model to predict the timing of the polar field reversals in the Northern and Southern hemispheres of the Sun. We also estimate the phase lag in the timing of the reversals between the two hemispheres.

We briefly discuss the AFT model used for our predictions and provide an outline for how we use our knowledge of past solar cycles to create synthetic AR catalogs with the observed patterns of AR emergence in section 2. In section 3 we presents our predictions of the timing of the hemispheric polarity reversal and the associated uncertainties based on different statistical techniques. Finally, in section 4 we summarize our findings.

## 2. SURFACE FLUX TRANSPORT MODEL

AFT, like other SFT models, solves the radial component of the induction equation to simulate the dynamics of the magnetic field on the surface of the Sun. The fundamental equation at the heart of the AFT is given by,

$$\frac{\partial B_r}{\partial t} + \vec{\nabla} \cdot (\vec{u}B_r) = S(\theta, \phi, t) + \eta \nabla^2 B_r, \quad (1)$$

Here,  $B_r$  is the radial component of magnetic field, and  $u$  is the horizontal components of the surface flows, which includes axisymmetric flows (differential rotation

and meridional flow) and convective flows (Hathaway & Rightmire 2011; Rightmire-Upton et al. 2012; Upton & Hathaway 2014a,b). The first term in the right hand side,  $S(\theta, \phi, t)$ , is the magnetic source term which represents new flux emergence at the solar surface. The second term,  $\eta \nabla^2 B_r$  (where  $\eta$  is diffusivity), is a diffusivity term added to stabilize the numerical scheme used in AFT and does not have any significant effect on the flux transport processes. See Upton & Hathaway (2014a,b) for additional details about the model.

AFT can be operated in two different modes: baseline mode and predictive mode. In baseline mode, AFT uses data assimilation of magnetograms to produce the synchronic maps, representing an accurate snapshot of the Sun’s entire photospheric magnetic field at a given time Upton & Hathaway (2014a,b). In predictive mode, AFT uses idealized bipolar ARs, to forecast the future evolution of the surface magnetic field. In the context of this letter, we create AFT Baseline maps by assimilating magnetograms from HMI up until 31st August, 2023. The Baseline map from 31st August, 2023 is then used as the initial condition to run the model further in time in the predictive mode. To run the AFT in predictive mode, we create ensembles of synthetic AR catalogs, based on the statistical properties of ARs and the timing and amplitude of previous solar cycles. ARs from these synthetic active catalogs are then incorporated into AFT as idealized bipolar magnetic ARs.

### 2.1. Synthetic Active Regions Generator (SARG)

To create synthetic AR catalogs, we use the Synthetic Active Regions Generator (SARG) code. To create a realization, SARG begins with the 13-month smoothed sunspot number v2.0 (Clette et al. 2016), taken from the Solar Influences Data Analysis Center (SIDC)<sup>1</sup>. This is used to set the cadence of spot emergence. Here, SARG defines the number of days between subsequent AR emergence as  $30.4368 / (0.3 + 0.269736 \times SSN)$ , where  $SSN$  is the sunspot number v2.0 for a given month. For each AR, SARG draws on a random sample from the KPVT/SOLIS BMR Flux log-normal distribution ( $\mu = 50.05$  &  $\sigma = 0.75$ ) of flux as described in Muñoz-Jaramillo et al. (2015, 2021). SARG randomly selects a hemisphere to place the spot and then determine the latitude of the AR by adding random fluctuations around the mean latitude location, which is given by the standard law for the equator-ward drift of the active latitudes as described in Hathaway (2011). The longitude of the AR is then drawn from a random uniform distri-

<sup>1</sup> Monthly sunspot data is taken from <https://www.sidc.be/SILSO/home>.

bution. SARG assigns the tilt of the AR based on the Gaussian distribution for Joy’s Law detailed in (Hale et al. 1919; Muñoz-Jaramillo et al. 2021). The tilt and the separation distance (Upton et al. 2023, in prep.) determines the relative position of the bipoles for each AR. The polarity of each bipole is assigned based on the Hale’s polarity law for that cycle and hemisphere (Stenflo & Kosovichev 2012). Due to the inherent randomness in the observed properties, no two SARG realizations will yield the exact same set of ARs, even though their statistical properties are identical. For each SARG realizations, we incorporate the ARs into AFT as bipolar Gaussian spot pairs with the specified properties (date, flux, polarity, and location).

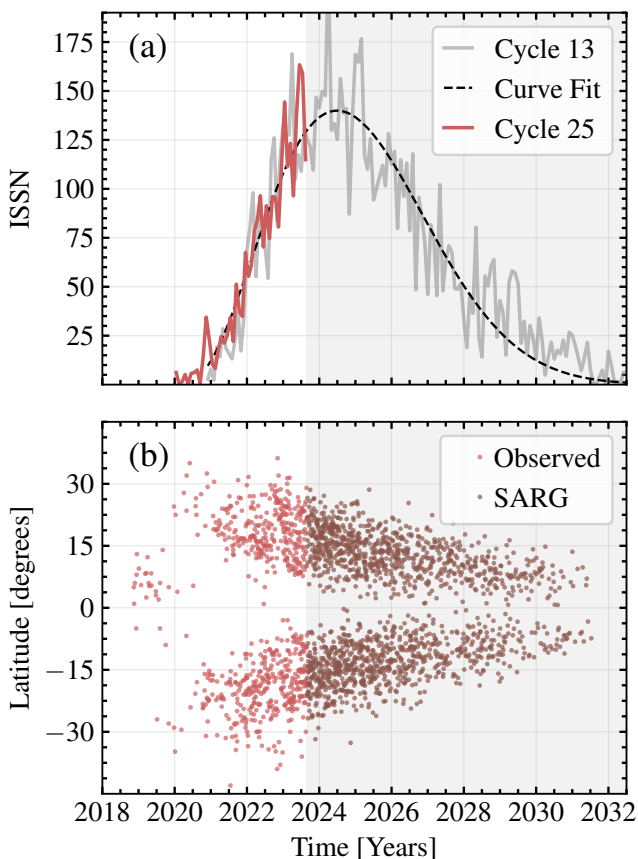


**Figure 1.** (a) The monthly average sunspot number for current cycle (Cycle 25), along with monthly average sunspot number for Cycle 13 and the best fit curve based on Hathaway et al. (1994). (b) shows the time latitude butterfly diagram for Cycle 25 up to August 2023 and one SARG realizations of synthetic ARs from September 2023 onward.

## 2.2. Selection of Past Solar Cycle

As discussed above, the selection ARs used for prediction is crucial. Here we base our SARG AR realizations

on a past solar cycle that most closely resembles the current progress of Cycle 25 (e.g., Hathaway & Upton 2016, who used Cycle 14 in place of Cycle 24). In Figure 1(a), we show the monthly averaged sunspot number v2.0 taken from the SIDC for Cycle 13 along with the current progress of Cycle 25. We fit an asymmetric curve (Hathaway et al. 1994; Hathaway 2011; Upton & Hathaway 2023) to the cycle and then shift it in time to match the timing of Cycle 25. As shown in Figure 1(a), Cycle 13 is an excellent match for Cycle 25 in terms of monthly averaged sunspot number. The butterfly diagram shown in Figure 1(b), further illustrates that the current cycle is closely following the SARG realization based on Cycle 13. This figure also illustrates that the frequency and distribution of ARs generated by SARG are qualitatively consistent with the observations. Hence, we select Cycle 13 as our reference cycle for SARG and produce 30 realizations of synthetic AR data. Simulating 30 different realizations in AFT highlights the potential variability due randomness inherent in the ARs. This allows us to characterize the uncertainty in our prediction of the polar field evolution.

## 3. RESULTS

Starting on September 1, 2023, we begin incorporating the SARG synthetic AR data into AFT and continue until the end of 2027. This process is repeated for all 30 SARG realizations. In Figure 2, we show a magnetic butterfly diagram from one realization. The dashed white line indicates the transition of AFT from the baseline mode to the predictive mode. This figure shows how residual flux in ARs is transported to the poles in streams of leading and following polarity flux. These streams drive the polar field evolution.

The polar field is often calculated as the average magnetic flux density in the polar caps (Upton & Hathaway 2014a). WSO measures the polar field with a single pixel, nominally above  $55^\circ$  latitude<sup>2</sup>, whereas HMI uses different latitude bands for this measurement, e.g.  $50^\circ - 90^\circ$  and  $60^\circ - 90^\circ$  (see Sun et al. 2015, for details). Here, we calculate the average polar fields above  $60^\circ$ . In Figure 3a and 3b we show the polar field for the Northern and Southern hemispheres respectively. The polar field strength for all 30 realizations are shown as light color lines. The mean polar field for all realizations is indicated by the darker lines. For reference, we also include the HMI polar field measurements (light gray).

<sup>2</sup> See Upton & Hathaway (2023) for a discussion on how the latitude range changes over the course of an orbit and the impact on the WSO polar field measurements.

We note that AFT shows excellent agreement with the HMI polar field.

We find no significant difference in the polar field of the 30 SARG realizations for nearly two years. This is expected as it typically takes a few years for the residual flux from the active latitudes to be transported to the poles. In [Figure 2](#) we see that a negative polarity flux stream begins to migrate to the North pole around 6 months before we stop data assimilation. This feature temporarily stalls the reversal of the Northern polar field. We note that this occurs in all of our simulations because the flux causing this unexpected behavior already exists on the Sun. Therefore, we can be confident that this will undoubtedly occur. While the Northern polar field stalls immediately, the Southern polar field initially continues its steady march toward reversal. However, we note that the ensemble of realizations do indicate that it may experience a brief stall of its own in 2024. This appears to be caused by a large concentration of negative flux in the active latitudes immediately before the assimilation process is stopped. While this will likely occur, it can be impacted by AR emergence in the coming months and is not as certain as the stalling of the Northern polar field.

As we progress further in time, differences in the polar field evolution across realizations become more apparent and the polar field evolution of our simulations continues to diverge. This is confirmation that the chaotic nature of flux emergence makes the task of predicting polar field evolution during solar maximum for more than a

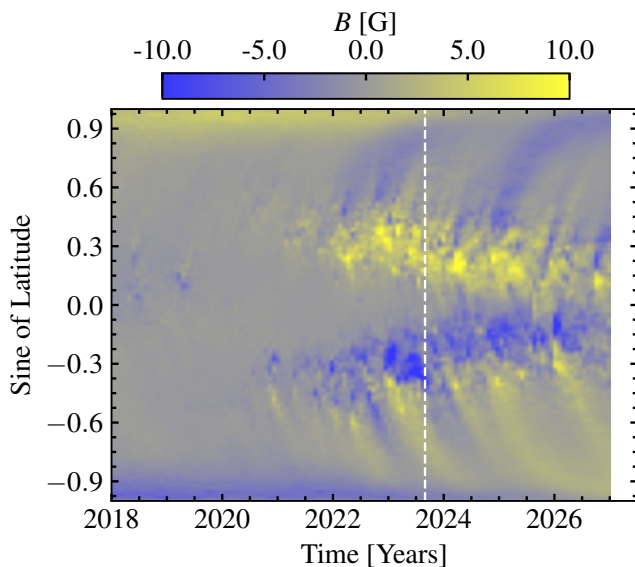


**Figure 2.** The magnetic butterfly diagram, constructed using AFT Baseline map till 31st August 2023 (marked using white dashed vertical line) and after that using one of the realizations of synthetic ARs in AFT’s predictive mode.

few years into the future is a challenging task ([Golubeva et al. 2023](#)). However, as we near the polarity reversal, we can expect less uncertainty in the predictions.

We now predict the of timing of polarity reversal in both the hemispheres by taking two different approaches, as discussed below.

### 3.1. Uncertainty Based on the Median Polar Field

We start by estimating the uncertainty in the timing of the reversal for the 30 different realizations used in this analysis. For each month, we compute the median polar field across all the realizations and calculate the first (Q1) and third (Q3) quartiles of the distribution. In [Figure 3c](#) and [3d](#), we show the temporal variation of this the polar field with 50% confidence intervals( between Q1 and Q3, indicated by shaded color regions). We use the timing of the reversal of these curves (Q1, median and Q3) to get the expected time of polarity reversal and associated uncertainty. These reversal times are marked by vertical lines. This approach suggests that the Northern hemisphere is most likely to undergo a polarity reversal between June 2024 and November 2024, with the median time in August 2024. Conversely, the Southern hemisphere is expected to experience a polarity reversal between November 2024 and August 2025, with the median in January 2025.

### 3.2. Uncertainty Based on the Individual Reversals

Next we discuss the second approach that we use to predict the timing of polarity reversal. Here we calculate the timing of the polarity reversal for each individual realization in both hemispheres. We then use the distribution of these individual reversal to estimate the timing of the polarity reversal and the associated uncertainties. In [Figure 4](#) we show the distribution of the timing for both hemispheres in the form of a violin plot, which is similar to the box plot (see [Stryjewski 2010](#), for details). This representation provides additional information about the probability distribution (shaded violin shaped region). Here, we use the Gaussian Kernel Density Estimator (KDE) to get the empirical probability distribution of the sample<sup>3</sup>. The extreme ends of the violins represent the range in the timing of polarity reversal based on our 30 realizations. Two dotted horizontal lines represent the first (Q1, 25th percentile) and third (Q3, 75th percentile) quartiles of the distribution. The solid lines represent the median of the distributions. After examining the distribution of timing, we find that the median is representative of the central tendency. There-

<sup>3</sup> See <https://matplotlib.org/stable/gallery/statistics/violinplot.html> for details about the violin plot.

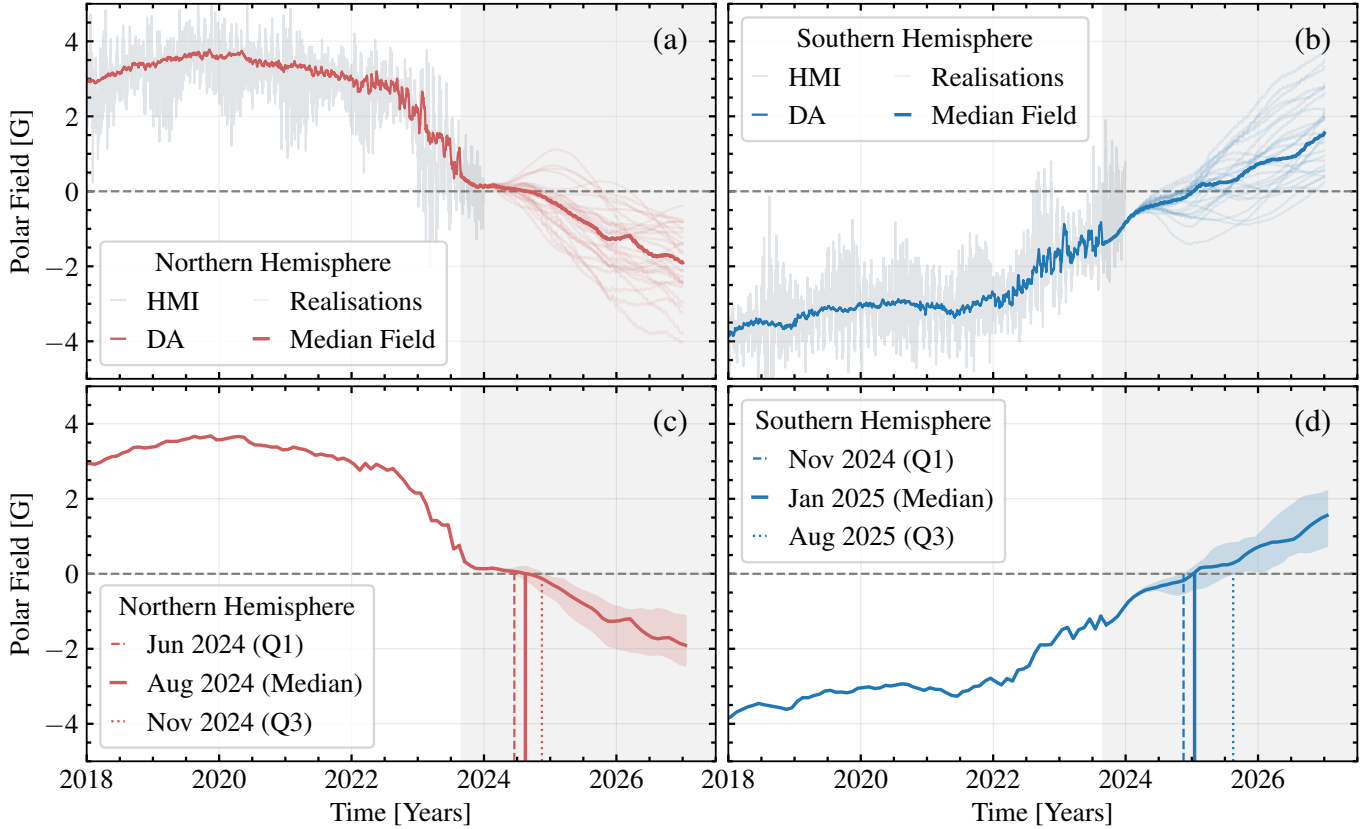


**Figure 3.** The polar field above  $60^\circ$  latitude for the (a) Northern and (b) Southern hemispheres is shown from the AFT Baseline through August 2023 (solid line), and for 30 SARG realizations afterward (light color lines). For reference, the HMI polar field above  $60^\circ$  is also shown (light gray). The median of the 30 realizations is indicated by the solid line after August 2023. The median polar field measurements for the Northern (c) and Southern (d) hemisphere are shown in the same manner. Here, the shaded color regions represent the 50% confidence interval between the first (Q1) and third (Q3) quartiles. The timing of the polar field reversal is marked by the vertical lines with the corresponding months noted in the legend.

fore, we use the median of the sample as our predictor and, Q1 and Q2 as our estimator of uncertainty for the timing of polarity reversal.

Based on the second approach, we predict that the Northern hemisphere is most likely to reverse its polarity in between June 2024 to November 2024 (50 percentiles), with median at August 2024. On the other hand, we predict that the Southern hemisphere will reverse its polarity sometime between November 2024 to July 2025 (50 percentiles), with median at February 2025. Using this approach, we also evaluate the distribution for the timing of axial dipole moment (ADM; see [Upton & Hathaway 2014a,b](#)) reversal. This indicates that the ADM is expected to change polarity in the middle of 2024. It's worth noting that the two distinct approaches used here exhibit good agreement in terms of the timing of polarity reversal, underlining that our predictions of polarity reversal timing is consistent and independent of the two methods.

As previously mentioned, different latitude limits can be used to calculate the polar fields. Therefore, we also

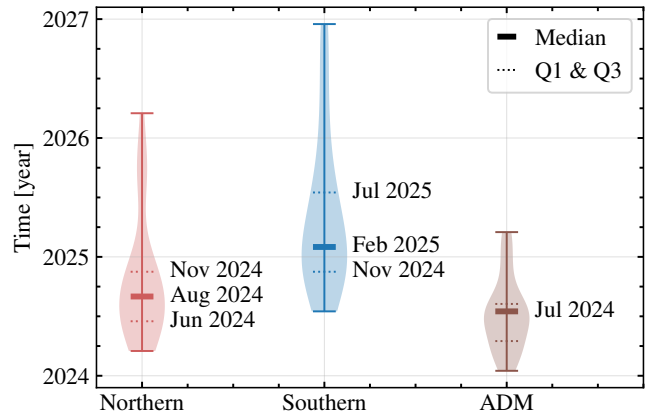


**Figure 4.** The violin plot shows the median timing of the polar field reversal, along with other statistical parameters such as the first (Q1) and third (Q3) quartiles, and the median timing of the reversal in the Northern (red) and Southern (blue) hemispheres. The third violin (brown) represents the distribution for the reversal of the axial dipole moment.

calculate the timing of polarity reversals using our sec-

ond approach with other latitude thresholds. In Table 1, we summarize the timing of polarity reversal for cases where lower latitude limits changes from  $50^\circ$  to  $75^\circ$  in increments of  $5^\circ$ .

#### 4. CONCLUSION

Understanding the evolution of the polar field in the near future is important for gaining insights into solar activity. For example, the timing of this polarity reversal can provide an estimate of when to expect solar maximum. Once the sign of the Sun’s polar field reverses polarity, the poles begin to build up magnetic flux of the opposite polarity, ultimately dictating the strength of the upcoming solar cycle. In this study we use the AFT model to predict the evolution of the polar field over the next few years. We simulate 30 realizations of synthetic ARs based on Solar Cycle 13 (which shows a good agreement with the current progress of Solar Cycle 25) as a proxy for the continued progression of the cycle. We use two different approaches to estimate the timing of polarity reversal in both hemispheres. Both approaches yield remarkably similar result in the prediction of the timing of the reversals. Consequently, we report the timing of polarity reversal based on the second approach, which uses the distribution of polarity reversal times across all 30 realizations.

By measuring the average polar field above  $60^\circ$ , we predict that for Cycle 25, the Northern hemisphere is likely to undergo a polarity reversal in August 2024 (with a 50% confidence range spanning from June to November 2024). The Southern hemisphere is expected to reverse its polarity in February 2025 (with a 50% confidence range from November 2024 to July 2025). Additionally, we conclude that for Cycle 25, the Northern hemisphere is expected to reverse its polarity  $\approx 5$  months before the Southern hemisphere, which is in line with the typical hemispheric lag. This is in stark contrast to Cycle 24, which was unusually asymmetric across the hemispheres and experienced a phase lag of approximately 16 months (Sun et al. 2015). Based on the assumption that the timing of the ADM reversal closely coincides with the time of solar cycle maximum,

we also conclude that we are approaching the Solar Cycle 25 maximum and we can expect that solar activity will likely begin to decline in the second half of the 2024. This is consistent with the timing of solar maximum very recently reported in Upton & Hathaway (2023) based on the precursors method and current progress of the Cycle 25. However (Jaswal et al. (2024) suggest that the timing of the ADM reversal may not coincide with cycle maximum.

The findings of this study are important for advancing our capability of making solar cycle predictions. The approaches used in this work for predicting the evolution of polar field and quantifying the uncertainty associated with it, are important for accessing and determining our ability to use SFT models to make reliable predictions about the evolution of the polar field. Furthermore, they serve as a demonstration of our current understanding of the solar cycle and solar dynamo processes. Evaluating the precision and accuracy of these results after the polar field reversals have come to pass will be essential for determining how the stochastic nature of active region emergence limits our fundamental ability to make long term (many years) predictions.

BKJ and LAU were supported by NASA Heliophysics Living With a Star Strategic Capabilities grant NNH21ZDA001N-LWSS and NASA grant NNH18ZDA001N-DRIVE to the COFFIES DRIVE Center managed by Stanford University. LAU was also supported by NASA Heliophysics Living With a Star grant NNH18ZDA001N-LWS. HMI data used in this study are courtesy of NASA-SDO and the HMI science team. The authors would also like to thank Andrés Muñoz-Jaramillo for his valuable suggestions and comments. This research has made use of NASA’s Astrophysics Data System (ADS; <https://ui.adsabs.harvard.edu/>) Bibliographic Services. We also thank the anonymous referees whose useful suggestions improved the overall quality of the paper.

*Software:* Matplotlib (Hunter 2007), Numpy (Harris et al. 2020) and Pandas (pandas development team 2020)

#### REFERENCES

- Babcock, H. D. 1959, ApJ, 130, 364, doi: [10.1086/146726](https://doi.org/10.1086/146726)
- Babcock, H. W. 1961, ApJ, 133, 572, doi: [10.1086/147060](https://doi.org/10.1086/147060)
- Bhowmik, P., Jiang, J., Upton, L., Lemerle, A., & Nandy, D. 2023, SSRv, 219, 40, doi: [10.1007/s11214-023-00983-x](https://doi.org/10.1007/s11214-023-00983-x)
- Bhowmik, P., & Nandy, D. 2018, Nature Communications, 9, 5209, doi: [10.1038/s41467-018-07690-0](https://doi.org/10.1038/s41467-018-07690-0)
- Charbonneau, P. 2010, Liv. Rev. Sol. Phys., 7, 3, doi: [10.12942/lrsp-2010-3](https://doi.org/10.12942/lrsp-2010-3)
- Clette, F., Cliver, E. W., Lefèvre, L., et al. 2016, SoPh, 291, 2479, doi: [10.1007/s11207-016-1017-8](https://doi.org/10.1007/s11207-016-1017-8)
- DeVore, C. R., Boris, J. P., & Sheeley, N. R., J. 1984, SoPh, 92, 1, doi: [10.1007/BF00157230](https://doi.org/10.1007/BF00157230)

Latitude	Northern Hemisphere			Southern Hemisphere		
	Q1	Median	Q3	Q1	Median	Q3
50°	Jan 2024	Apr 2024	Jun 2024	Nov 2023	Feb 2024	Dec 2024
55°	Feb 2024	Apr 2024	Aug 2024	May 2024	Sep 2024	Apr 2025
60°	Jun 2024	Aug 2024	Nov 2024	Nov 2024	Feb 2025	Jul 2025
65°	Oct 2024	Feb 2025	Apr 2025	Apr 2025	Sep 2025	Feb 2026
70°	Feb 2025	May 2025	Aug 2025	Aug 2025	Dec 2025	Jul 2026
75°	May 2025	Aug 2025	Nov 2025	Nov 2025	Apr 2026	Nov 2026

**Table 1.** The various statistical parameters for the timing of reversal of polar field for multiple latitude limits. Here, Q1 and Q3 represents the first and third quartiles of the distribution, respectively.

- Golubeva, E. M., Biswas, A., Khlystova, A. I., Kumar, P., & Karak, B. B. 2023, MNRAS, 525, 1758, doi: [10.1093/mnras/stad2254](https://doi.org/10.1093/mnras/stad2254)
- Hale, G. E., Ellerman, F., Nicholson, S. B., & Joy, A. H. 1919, ApJ, 49, 153, doi: [10.1086/142452](https://doi.org/10.1086/142452)
- Harris, C. R., Millman, K. J., van der Walt, S. J., et al. 2020, Nature, 585, 357, doi: [10.1038/s41586-020-2649-2](https://doi.org/10.1038/s41586-020-2649-2)
- Hathaway, D. H. 2010, Living Reviews in Solar Physics, 7, 1, doi: [10.12942/lrsp-2010-1](https://doi.org/10.12942/lrsp-2010-1)
- . 2011, SoPh, 273, 221, doi: [10.1007/s11207-011-9837-z](https://doi.org/10.1007/s11207-011-9837-z)
- Hathaway, D. H., & Rightmire, L. 2011, ApJ, 729, 80, doi: [10.1088/0004-637X/729/2/80](https://doi.org/10.1088/0004-637X/729/2/80)
- Hathaway, D. H., & Upton, L. A. 2016, Journal of Geophysical Research (Space Physics), 121, 10,744, doi: [10.1002/2016JA023190](https://doi.org/10.1002/2016JA023190)
- Hathaway, D. H., Wilson, R. M., & Reichmann, E. J. 1994, SoPh, 151, 177, doi: [10.1007/BF00654090](https://doi.org/10.1007/BF00654090)
- Hunter, J. D. 2007, Computing in Science & Engineering, 9, 90, doi: [10.1109/MCSE.2007.55](https://doi.org/10.1109/MCSE.2007.55)
- Jaswal, P., Saha, C., & Nandy, D. 2024, MNRAS, 528, L27, doi: [10.1093/mnras/528/L27](https://doi.org/10.1093/mnras/528/L27)
- Jha, B. K., Karak, B. B., Mandal, S., & Banerjee, D. 2020, ApJL, 889, L19, doi: [10.3847/2041-8213/ab665c](https://doi.org/10.3847/2041-8213/ab665c)
- Jiang, J., Hathaway, D. H., Cameron, R. H., et al. 2014, SSRv, 186, 491, doi: [10.1007/s11214-014-0083-1](https://doi.org/10.1007/s11214-014-0083-1)
- Muñoz-Jaramillo, A., Navarrete, B., & Campusano, L. E. 2021, ApJ, 920, 31, doi: [10.3847/1538-4357/ac133b](https://doi.org/10.3847/1538-4357/ac133b)
- Muñoz-Jaramillo, A., Sheeley, N. R., Zhang, J., & DeLuca, E. E. 2012, ApJ, 753, 146, doi: [10.1088/0004-637X/753/2/146](https://doi.org/10.1088/0004-637X/753/2/146)
- Muñoz-Jaramillo, A., Senkpeil, R. R., Windmueller, J. C., et al. 2015, ApJ, 800, 48, doi: [10.1088/0004-637X/800/1/48](https://doi.org/10.1088/0004-637X/800/1/48)
- pandas development team, T. 2020, pandas-dev/pandas: Pandas, latest, Zenodo, doi: [10.5281/zenodo.3509134](https://doi.org/10.5281/zenodo.3509134)
- Rightmire-Upton, L., Hathaway, D. H., & Kosak, K. 2012, ApJL, 761, L14, doi: [10.1088/2041-8205/761/1/L14](https://doi.org/10.1088/2041-8205/761/1/L14)
- Scherrer, P. H., Schou, J., Bush, R. I., et al. 2012, SoPh, 275, 207, doi: [10.1007/s11207-011-9834-2](https://doi.org/10.1007/s11207-011-9834-2)
- Schrijver, C. J., & Title, A. M. 2001, ApJ, 551, 1099, doi: [10.1086/320237](https://doi.org/10.1086/320237)
- Stenflo, J. O., & Kosovichev, A. G. 2012, ApJ, 745, 129, doi: [10.1088/0004-637X/745/2/129](https://doi.org/10.1088/0004-637X/745/2/129)
- Stryjewski, L. 2010, <https://api.semanticscholar.org/CorpusID:36975036>
- Sun, X., Hoeksema, J. T., Liu, Y., & Zhao, J. 2015, ApJ, 798, 114, doi: [10.1088/0004-637X/798/2/114](https://doi.org/10.1088/0004-637X/798/2/114)
- Svalgaard, L., Cliver, E. W., & Kamide, Y. 2005, Geophys. Res. Lett., 32, L01104, doi: [10.1029/2004GL021664](https://doi.org/10.1029/2004GL021664)
- Svalgaard, L., & Kamide, Y. 2013, ApJ, 763, 23, doi: [10.1088/0004-637X/763/1/23](https://doi.org/10.1088/0004-637X/763/1/23)
- Upton, L., & Hathaway, D. H. 2014a, ApJ, 780, 5, doi: [10.1088/0004-637X/780/1/5](https://doi.org/10.1088/0004-637X/780/1/5)
- . 2014b, ApJ, 792, 142, doi: [10.1088/0004-637X/792/2/142](https://doi.org/10.1088/0004-637X/792/2/142)
- Upton, L., Ugarte-Urra, I., & Warren, H. P. 2023
- Upton, L. A., & Hathaway, D. H. 2023, arXiv e-prints, arXiv:2305.06516, doi: [10.48550/arXiv.2305.06516](https://doi.org/10.48550/arXiv.2305.06516)
- Upton, L. A., & Hathaway, D. H. 2023, Journal of Geophysical Research: Space Physics, 128, e2023JA031681, doi: <https://doi.org/10.1029/2023JA031681>
- van Ballegooijen, A. A., Cartledge, N. P., & Priest, E. R. 1998, ApJ, 501, 866, doi: [10.1086/305823](https://doi.org/10.1086/305823)
- Wang, Y. M., Nash, A. G., & Sheeley, N. R., J. 1989, ApJ, 347, 529, doi: [10.1086/168143](https://doi.org/10.1086/168143)
- Yeates, A. R., Cheung, M. C. M., Jiang, J., Petrovay, K., & Wang, Y.-M. 2023, SSRv, 219, 31, doi: [10.1007/s11214-023-00978-8](https://doi.org/10.1007/s11214-023-00978-8)